Journal of the Oceanographical Society of Japan
Vol. 44, pp. 143 to 156, 1988

Turbulent Structure in Water under Laboratory Wind Waves*

Ikuo Yoshikawa¶, Hiroshi Kawamura†, Kuniaki Okuda‡
and Yoshiaki Toba†

Abstract: The structure of the turbulent boundary layer underneath laboratory wind waves was studied by using a combination of a high-sensitivity thermometer array with a two-component sonic flowmeter. The temperature fluctuations are used to detect movements of water parcels, with temperature as a passive quantity. The turbulence energy was dominant in the frequency range ($0.01 \sim 0.1$ Hz), which was much smaller than the wind-wave frequency ($2 \sim 5$ Hz), and in which the turbulence was anisotropic. There was a frequency range ($0.2 \sim 2$ Hz for velocity, $0.2 \sim 5$ Hz for temperature fluctuation) where the turbulence was isotropic and had a $-5/3$ slope in the energy spectrum. These points are the same as those in previous works. However, by analyses of the time series by using a variable-interval time-averaging technique (VITA), it has been found that conspicuous events in this main turbulence energy band are the downward bursting from the vicinity of the water surface. Thus the structure of the water layer underneath the wind waves has characters which are similar to the familiar turbulent boundary layer over a rough solid wall, as already conceived. It has been found that, at the same time, the turbulence energy can be related to quantities of the wind waves (the root mean squared water level fluctuation and the wave peak frequency), for different wind and wave conditions. That is, the turbulence underneath the wind waves develops under a close coupling with the wind waves.

1. Introduction

As to the turbulence structure in water underneath wind waves, the following aspects have already been reported (*e.g.*, Jones and Kenney, 1977; Donelan, 1978; Csanady, 1984; Jones, 1985; Mitsuyasu and Kusaba, 1985; Terray and Bliven, 1985; Wang and Wu, 1985); that most of the enegy of turbulence is contained in frequency regions lower than the wind-wave frequencies, that the downward momentum flux is performed in these regions, that there also exists an inertial subrange where the spectral density of velocity fluctuation has a slope of -5/3-power of frequency, and that the friction velocity scaling law is satisfied which is similar to that of the turbulent boundary layer above a solid wall. In the present study, an experiment was carried out in order to elucidate characteristics of the large scale structure of turbulence in the low frequency regions, and also their relationship with wind waves.

The wind wave is a special phenomenon which is generated by the wind at the air-water interface. In wind waves, not only elements of water waves but, in addition, elements of wind drift and turbulence in the air and water boundary layers are important in its dynamics. A decade of research into various aspects of wind drift and turbulence in the wind wave by using flow visualization techniques in the author's laboratory

* Received 16 September 1987; in revised form 18 April 1988; accepted 18 April 1988.
† Department of Geophysics, Faculty of Science, Tohoku University, Sendai, 980 Japan.
¶ Present affiliation: Kobe Marine Observatory, Kobe, 650 Japan.
‡ Tohoku Regional Fisheries Research Laboratory, Shiogama, 985 Japan.

was reviewed by Toba (1985). For the present paper, a detailed investigation was performed by using a combination of a two-component sonic flowmeter and temperature sensors, and a close relationship of the turbulence with the wind wave is reported. As will be reported elsewhere (Toba, 1988), this relationship is interpreted as another aspect of the local equilibrium between the wind and the wind wave, where the similarity laws of wind waves as represented by the 3/2-power law exist.

In this study, we first observe the large-scale structure in the turbulent boundary layer under wind waves. According to recent studies of turbulence, ordered motions in the boundary layer over flat walls have their original energy source in the vicinity of the walls (Cantwell, 1981). For turbulent air flow over wind waves, Kawamura and Toba (1985) have shown that the origin of turbulence energy may be a shear layer separated at the edge of separation bubbles which were formed behind some individual wave crests. Okuda (1982) showed the existence of a high vorticity layer in the water near the crest of the wind waves. The vorticity layer had a streamwise velocity which was close to the phase speed of the dominant wind waves, and moved downstream together with the individual crests of wind waves. Okuda (1982) reported that the water particles near the crest sometimes intruded downward, even though there was no air entrainment. Referring to experimental works concerning the reattachment of separated shear flow, Csanady (1985) and Kawamura and Toba (1988) pointed out the possibility of a direct dynamical interaction between the air flow and the wind waves producing a high vorticity layer in the backward face near the wave crest, where the separated air flow reattaches. We speculate that the energy source of the water turbulence is in the water very close to the water surface organized as the high vorticity layer.

In order to recognize ordered motions randomly occurring in a turbulent boundary layer over a flat plate, Chen and Blackwelder (1978) used temperature as a passive scalar. This means that a small temperature variation does not have any dynamical influence in the flow system. In the present experimental situation, the active air-water interaction at the water surface causes latent heat flux toward the air as well as momentum flux to the water. We have thus used the temperature to detect the water originating from the surface by measuring small temperature variations. By a combination of the temperature sensors and the sonic flowmeter, a large scale nature of the turbulence at energy containing frequencies will be revealed (Section 3).

On the basis of the physical concept of the large-scale structure of turbulence (*i.e.* the ordered motion) developed in Section 3, statistical features of the energy containing turbulence is extracted, and evidence is presented that there is a close relationship between wind waves and the turbulence in water underneath the wind waves (Section 4).

2. Experiments

Experiments were carried out using one of wind-wave tunnels of Tohoku University. The tunnel is 20 m long, 0.6 m wide and 1.2 m high with 0.67 m deep water (Fig. 1). We used three reference wind speeds which were measured at the entrance of the tunnel: Ur=5.0 m sec^{-1}, 7.7 m sec^{-1} and 9.1 m sec^{-1}, hereafter designated as U1, U2 and U3, respectively.

A sonic flowmeter, which has two pairs of transmitters 2.6 cm apart, was placed at Fetch= 8.2 m to measure water velocity components under the wind waves: u in the streamwise (x) and w in the upward (z) directions. The sonic flowmeter has a frequency response up to 20 Hz, which is sufficient sensitivity for the measure-

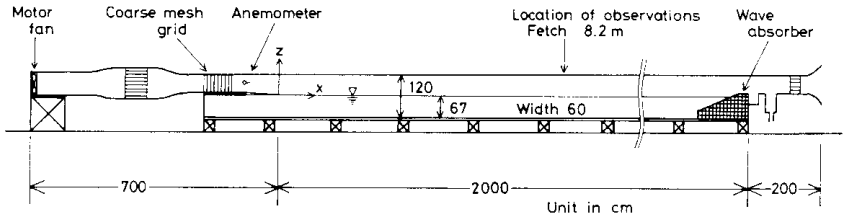

Fig. 1. A schematic picture of the wind wave tunnel.

ment of water turbulence under the wind waves. The flowmeter was traversed vertically to measure the velocity fluctuations at 13 depths ranging $z=-1.9$ to -30 cm (z was measured upward from the water surface at rest) for each of the wind speeds. Two capacitance-type wave-gauges were used to measure surface displacement η. One of them was located at the same fetch as the flowmeter and the other at a fetch 3 cm downstream. The signals from the flowmeter at each of the depths were recorded on an analogue magnetic tape recorder, together with the signals from the wave gauges, for 10 min. The voltage signals on the tape recorder were converted to digital with a sampling rate of 50 Hz.

Besides the above mentioned experiments, a specially designed experiment was conducted in order to observe characteristic features of the turbulent motions. The flowmeter was placed at $z=-7.2$ cm under the wind U2. Three thermistor thermometers with high sensitivity and quick response were used to detect small temperature fluctuations, smaller than 0.01°C, caused by sensible-heat loss at the water surface. The thermistors were plased at $z=-1.5$, -3.5 and -7.2 cm, and the temperature fluctuations obtained were designated as θ_1, θ_2 and θ_3, respectively. As will be shown in the results and discussed later, the small variations in temperature are closely connected with downward intrusion of water masses that have higher streamwise velocity (having larger momentum). The thermometer was composed of a thermistor enclosed in a rod 0.7 mm in diameter and 4 mm in length (Fig. 2), and a bridge circuit. To record the thermistor signals corresponding to the small temperature fluctuations, a high-gain instrumentation amplifier and a low-pass filter with a cut-off frequency of 25 Hz were used. The time-constant τ, showing the frequency response of the whole system of the thermometer, was about 0.07 sec for a sudden change of temperature. This is a sufficient response for the measurement of temperature variations associated with water turbulent fluctuations of the water.

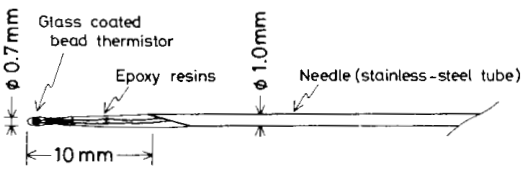

Fig. 2. A thermistor probe.

The linearity of the thermistor output was achieved within an error oi 0.12% for a range of ±0.1°C around a temperature set before the experiment. We adjusted the equilibrium point of the bridge circuit against the expected trend of the water temperature change in order to avoid saturation of the output-voltage signal. Since the trend was caused by heat flux toward the air at the water surface, the water temperature had a tendency to decrease. This temperature decrease was continually monitored by another thermistor, which had a rather low-frequency ($\tau=0.18$ sec) and linear response for a 1°C temperature range. The monitored trend of the water temperature was subtracted from the output of the three sensitive-thermistor thermometers to obtain purely fluctuating components of the temperature. The three thermistors were placed at the same fetch as the flowmeter, and the thermistor for the temperature trend at a depth 2.5 cm at Fetch = 8.85 m. The air temperature and the humidity were also monitored during the experiment. The signals of the flowmeter, the three thermistor thermometers and the wave gauges were recorded on

Table 1. Parameters characterizing the winds and the wind waves for each of the three wind conditions. Ur: reference wind speed, u_*: friction velocity, $(\overline{\eta^2})^{1/2}$: standard deviation of the surface displacement, f_p: the spectral peak frequency of the wind wave, σ_p: $2\pi f_p$, λ_p: wavelength of the spectral peak wind wave, $\lambda(\sigma_p)$: wavelength of the peak wind wave calculated from f_p by applying the dispersion relation of surface gravity waves.

Run	Ur (cm sec^{-1})	u_* (cm sec^{-1})	$(\overline{\eta^2})^{1/2}$ (cm)	f_p (Hz)	σ_p (sec^{-1})	λ_p (cm)	$\lambda(\sigma_p)$ (cm)
U1	5.0	21.4	0.227	4.15	26.1	12.6	9.05
U2	7.7	35.8	0.460	3.00	18.0	22.6	17.31
U3	9.1	36.9	0.660	2.78	17.5	28.4	20.20

a tape recorder for 40 min. The monitored trend of the water temperature showed a linear decrease of 0.05°C from the start to the end of the experiment.

Table 1 shows the parameter characterizing the winds and the wind waves under the three wind conditions. The friction velocity u_* of the air was determined from the mean velocity profiles of the air flow, applying the logarithmic law for the velocity profile, with the von Kármán constant of 0.4. The wavelength λ_P for the wind waves of the spectral peak frequency f_P was determined by calculating the phase difference between the signals of two wave-gauges. Another wavelength $\lambda(\sigma_P)$ is also shown, which was obtained from f_P by applying a dispersion relation of the deep water gravity wave.

Figure 3 shows the mean water velocity profiles for each of the wind speeds. Surface drift currents, in the streamwise direction, are concentrated in the upper layer above $z=-10$ cm for the three wind cases. As will be shown later, these layers correspond with the layers containing energetic turbulence whose energy is supplied from air flow through the wind and wind-wave dynamics. The main purpose of the present study is to investigate the structure of turbulence associated with this dynamic process, to understand how turbulence is generated and maintained under the wind waves.

In the layer deeper than $z=-10$ cm, there is a reverse flow to supplement the mass flux caused by the streamwise drift current in the upper layer. It will be shown later that the intensity of the turbulence and Reynolds stress in the deeper layer are small in comparison with those in the upper layer. Since the Reynolds stress is especially small, the turbulence in the deeper layer is considered to be isotropic. One may expect some interactions between the streamwise drift layer and the reverse flow at about $z=-10$ cm. However, since the turbulence in the upper layer, which we intend to observe, is most energetic in the whole water layer, we consider that the structure of turbulence in the surface boundary layer is not much affected by the reverse flow except near the depth very close to the boundary with the reverse flow.

In Fig. 3, since the streamwise velocity profiles have some ambiguity in determining the lines for the logarithmic profiles, the values of

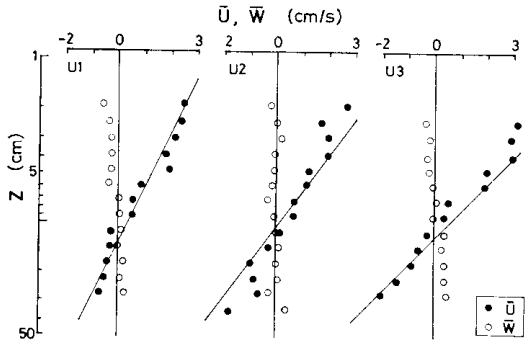

Fig. 3. Mean velocity profiles.

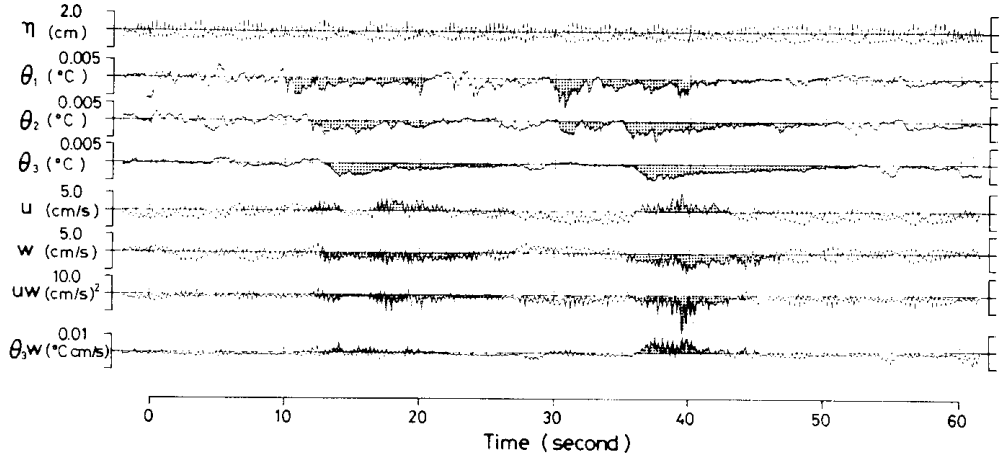

Fig. 4. An example of a set of time series of the fluctuations obtained by the experiment using a wave gauge, three thermistors and a two-component sonic flowmeter, and of the vertical momentum and heat fluxes.

the friction velocity of the water u_{*w}, which were estimated from the data shown in Fig. 11, were used to draw the lines. This point will be described in more detail in Section 4.

3. Large-scale structure in turbulent shear flow below wind waves

3. 1. Characteristics of large-scale structure in time series

Figure 4 shows an example of a set of the time series obtained by experiment. The surface displacement η at the same fetch as the flowmeter, the temperature fluctuations θ_1, θ_2 and θ_3, and the velocity fluctuations (u, w) are shown together with the instantaneous Reynolds stress $u \times w$ and the instantaneous heat flux $\theta_3 \times w$ at $z=-7.2$ cm. The time series of the products of the fluctuating components such as $u \times w$ and $\theta_3 \times w$ have often been used to recognize organized structure in the turbulent boundary layers (*e.g.*, Cantwell, 1981; Antonia, 1981; Kawamura *et al.*, 1981).

In the velocity signals, orbital motions of the wind waves are superimposed on slowly varying fluctuations. In contrast, effects of the orbital motions are not seen in the temperature fluctuations, which means that there is no significant thermal stratification in the water. Large-scale variations on an order of 10 sec in the temperature fluctuations are seen, however, at every depth. Their amplitudes are about 2×10^{-3}°C, as seen in the figure. The trend of the water temperature, which was 0.05°C for 40 min (-2.1×10^{-5}°C sec^{-1}), is negligible when compared with the amplitude of the large-scale variations. The variations at three depths take place synchronously (see shaded areas in Fig. 4), and show a tendency to start with a sudden decrease of temperature and then recovering gradually to the mean values. The sudden temperature decrease suggests the passage of an internal temperature front. The slightly colder water parcel is supposed to be generated in a thin layer of the air-water interface by evaporation, and it intrudes forming an ordered motion into the water layer in which there is no significant thermal stratification, as will be investigated in 3.2.

When the variations in θ_3 appear, large-scale downward motions ($w<0$) coupled with larger streamwise velocity ($u>0$) are seen at the same depth. The second event is especially prominent in Fig. 4, where the event produces larger instantaneous Reynolds stress and heat flux. In the following two sections, we will examine these large-scale fluctuations in detail using two different methods of analyses.

3. 2. VITA analysis of large-scale structure

In order to sample randomly occuring events from the measured turbulence signals according to detection criteria, and to obtain ensemble-averaged features of the events, a variable-interval time-averaging technique (VITA) is used in the filed of turbulence study (Antonia, 1981; Cantwell, 1981).

VITA was first proposed by Blackwelder and Kaplan (1976), who investigated rapid changes in the velocity signals associated with bursting phenomena in the turbulent boundary layer over a wall. Chen and Blackwelder (1978) have explored the turbulent boundary layer by using temperature as a passive contaminant: a temperature tracer was introduced into the flow field by heating the wall in their case. They adopted the VITA technique with minor modifications for the detection of a rapid change in the temperature signal.

The experimental situation on the present study is similar to that of Chen and Blackwelder. In both cases, the temperature variation can be used as an obvious manifestation of the large-scale turbulence structure although the sources of the heat are different. In the present case, the (negative) heat source is the latent heat flux toward the air, which takes place at the water surface. The source of the momentum, which generates and maintains the water turbulence, is in the air flow, and the momentum is transfered to the water also through the water surface. The temperature variations are detectable but too small to produce bouyancy forces, so the temperature behaves as a passive scalar in our case. The large-scale temperature decrease starting with a rapid change is considered to be a manifestation of the intrusion of a fluid parcel originated from the water surface.

We employ VITA to the quantity $\theta(t)$ according to the detection criterion by Chen and Blackwelder (1978). The identification of the rapid change is performed whenever the two conditions $\overline{\theta^2}-\bar{\theta}^2>k\theta^2_{rms}$ and $\dot{\bar{\theta}}<0$ are satisfied,

where θ_{rms} is the root mean square of the quantity, k is a threshold value, the dot denotes differentiation with respect to time, and the overbar denotes averaging over a time interval τ_d. Therefore, for example

$$\overline{\theta^2}-\bar{\theta}^2=\frac{1}{\tau_d}\left[\int_{t-\tau_d/2}^{t+\tau_d/2}\theta^2(t)dt-\left(\int_{t-\tau_d/2}^{t+\tau_d/2}\theta(t)dt\right)^2\right].$$

The values of the parameters k and τ_d used here are 1.0 and, 3.0 sec, respectively, which were selected, after some trial analyses, as suitable for detecting the sudden temperature decrease in the present case. Once the reference times t_n, taken at the midpoint of the events detected by VITA, were determined, an ensemble average of θ can be calculated as

$$\langle\theta(t)\rangle=\frac{1}{N}\sum_{n=1}^{N}\theta(t_n+t), \qquad (3.1)$$

where N is the total number of detected events. The ensemble averages of the other signals obtained simultaneously with θ are also defined in the same way as Eq. (3.1).

Figure 5 shows the results of the ensemble averages of θ_1, θ_2, θ_3, u, w, $u\times w$ and $\theta_3\times w$. As the detection signal, θ_3 was used, and $t=0$ in Fig. 5 shows the time when the events (*i. e.* the sudden decrease of θ_3) were identified.i Sxty-one events were detected during forty minutes. Corresponding to the sudden decrease of θ_3, there were large-scale velocity fluctuations at the same depth. During $t=0\sim10$ sec, the positive streamwise velocity coupled with the downward component produced large Reynolds stress, and the downward velocity and the negative θ_3 produced large upward heat flux at $z=-7.2$ cm. This feature means that the conditionally sampled fluid (appearing $t=0\sim10$ sec) comes down to this depth, possessing an excess of streamwise momentum and low temperature, which agrees with the concept of momentum and heat transfer from the surface into the water boundary layer in the wind wave field. Sudden decreases are also seen in θ_1 and θ_2, and the shallower the depth is, the earlier the decreases appear.

Assuming that a large-scale ordered motion, penetrating across the layers at the three depth, causes these systematic variations in temperature and velocity as shown in Fig. 5, we propose a schematic picture of the ordered motion as shown in Fig. 6. The characteristic speed of the low temperature water mass detected at $z=-7.2$ cm is used to represent the speed of the internal front through the layer of $z=-1.5\sim-7.2$ cm.

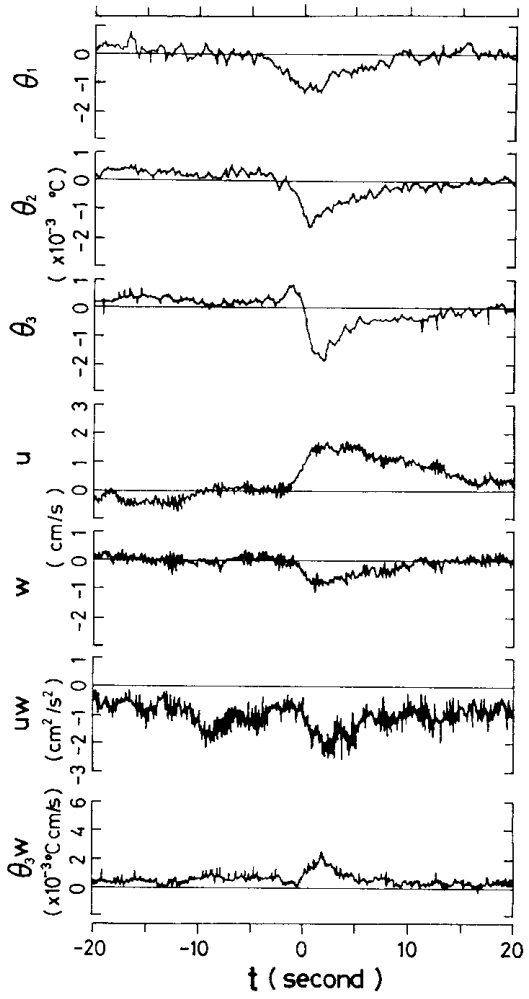

Fig. 5. Results of VITA analysis (see the text).

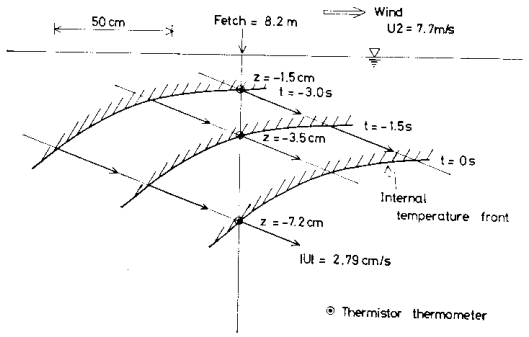

Fig. 6. Schematic picture of the ordered motion in the water turbulent boundary layer.

Considering the detection times of the sudden decrease at the three depths, a configuration of the internal front is conjectured. This configuration resembles the front pattern which Chen and Black welder (1978) obtained by using a composite picture of the two-dimensional velocity field associated with the temperature front, although we should be careful about the differences; the location of the turbulence energy source and the streamwise direction differ between their experimental situation and the present.

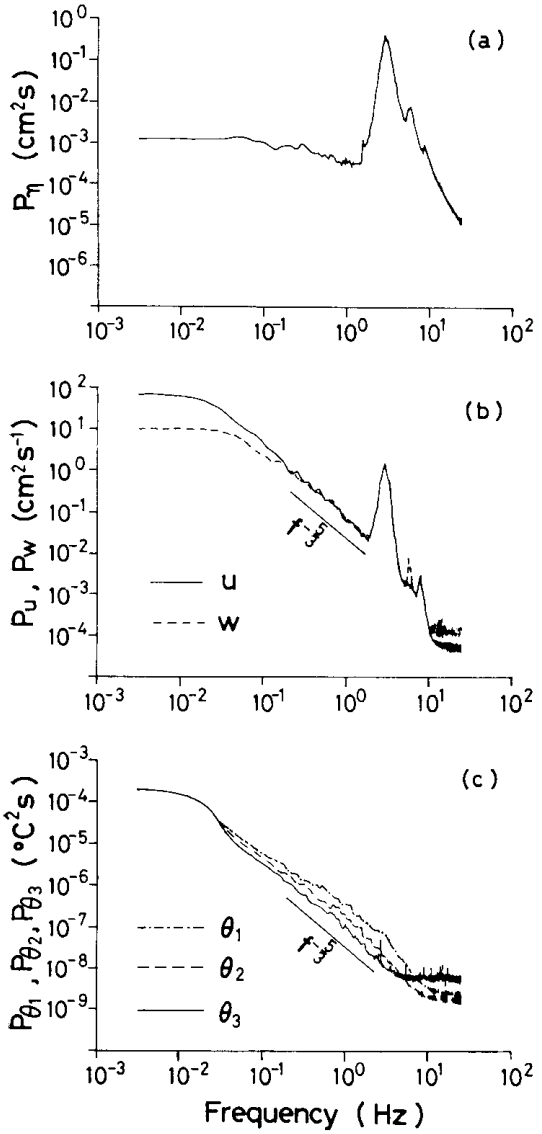

Fig. 7. (a) Power spectrum of surface displacement, (b) power spectra of water velocities u, w and (c) power spectra of temperature fluctuations θ_1, θ_2, and θ_3. The wind condition is $U2$.

3.3. Spectral features of large scale structure

Power spectra of the surface displacement η, the velocities at $z=-7.2$ cm and the temperature fluctuations θ_1, θ_2, θ_3 are shown in Fig. 7. To investigate spectral features in a wide frequency range of 0.001~25 Hz, each of the spectra was derived as an ensemble average of six spectra, each of which was calculated from 16,384 data points.

The wind-wave spectrum shows the characteristic shape of laboratory wind waves, with a peak frequency at 3.0 Hz. The orbital velocity appears as the obvious peaks in the velocity spectra. However, the temperature spectra show no influence of the wind waves, because there is no significant stratification in the water, as inferred in section 3.1. This situation seems very natural, if we consider that the amplitude of the orbital motion is very small in the field of no significant thermal stratification. Since the temperature can be considered as a passive scalar in this case, the main mechanism responsible for causing the temperature variation is advection due to large scale turbulence in water.

As can be seen in Figs. 7(b) and (c), both the spectra of velocity and temperature have $-5/3$ slopes in a frequency range of 0.2~2 Hz. In a frequency range lower than 0.2 Hz, the spectral density of velocity and temperature increase as frequency decreases. The temperature spectra has a structure similar to the velocity spectra except for the vicinity of the wind-wave peak frequency. The turbulence energy is mainly contained in the frequency range lower than the peak frequency of the wind waves. Since the $-5/3$ slopes in the spectra of velocity and temperature can be considered to show an inertia subrange of the local isotropic turbulence, we may expect that the turbulence energy source exist in the frequency range lower than the frequency range of $-5/3$ slope.

Figure 8 shows the cospectrum of u and w multiplied by frequency, $f \cdot C_{uw}$ to evaluate the contribution of the frequency components to the Reynolds stress production at $z=-7.2$ cm. The

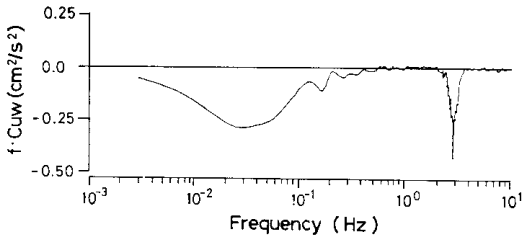

Fig. 8. Contribution of the frequency components to the Reynolds stress production.

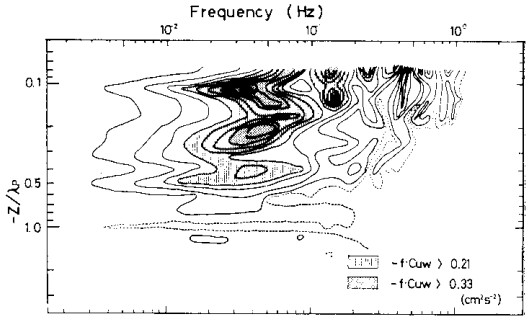

Fig. 9. Distribution of $-f \cdot C_{uw}$ in the frequency-depth domain.

major contribution (about 90%) is made in the frequencies much lower than the peak frequency of the wind waves, and there is a peak of $f \cdot C_{uw}$ in a frequency range (0.01～0.1 Hz) which is lower than the range of $-5/3$ slope.

It is apparent that the velocity spectra of Fig. 7(b) are partly similar to the spectra obtained by Donelan (1978), Mitsuyasu and Kusaba (1985), Terray and Bliven (1985) and Wang and Wu (1985). The existence of the $-5/3$ slope range, which is located at the lower frequencies, seems to be common for data taken in wind-wave tanks. The frequency range of 0.5～2 Hz represents the range of homogeneous turbulence as seen also in Fig. 7. Since the temperature spectra of Fig. 7(c) have the $-5/3$ slope range which extends to cover the wind-wave frequency range, there is a possibility that the turbulence components of the velocity may also be extended with the $-5/3$ slope into the wind-wave frequency range. Another peak of $f \cdot C_{uw}$ at the wind-wave peak frequency in Fig. 8 seems to be due to the interaction between the orbital motion and turbulence at the peak frequency, as Kitaigorodskii *et al.* (1983) also pointed out.

In order to investigate the major contributor to the Reynolds stress production in the whole turbulent boundary layer, cospectra were calculated by using the velocity fluctuations measured at other 13 depths under the wind condition U2. In this case, spectrum at each depth was calculated from one set of 16,384 data points. Figure 9 shows contours of $-f \cdot C_{uw}$ in a frequency-depth (normalized by λ_p) domain. The structure of $-f \cdot C_{uw}$ in the frequencies higher than 0.1 Hz decreases with depth increases. However, the peaks of $-f \cdot C_{uw}$ in the range of 0.01～0.1 Hz, as shown in Fig. 9, are commonly observed from the shallowest depth to a depth of about $z \sim 0.5\lambda_p$. We infer that the Reynolds stress production in the frequency range 0.01～0.1 Hz is made by a large-scale structure extending across the considerable depths of the turbulent boundary layer. Here, as another appearance of this process contributing to the Reynolds stress production, we can recall the large-scale structure, having a time scale of ～10 sec, as detected by VITA in the previous scetion.

We consider that the major process contributing to the Reynolds stress production as well as the large-scale structure recognized by VITA indicates an ordered motion, which exists in the water turbulent boundary layer, and which is a counterpart of the ordered motion investigated by Kawamura and Toba (1985) in the air flow over the wind waves. As a matter of fact, Kawamura and Toba (1988) reported that there is an intermittent large momentum flux in the boundary layer above the laboratory wind waves, and that this event is related to the air-flow separation behind the wave crests and the bursting of low-speed air masses in the separation bubbles. Underneath the wind waves, there is also an intermittent recirculation flow below the wave crests as reported by Toba *et al.* (1975) for breaking wind waves and by Okuda (1982) for non-breaking wind waves. This recirculation can be interpreted as the counterpart of the air-flow separation behind the crests. The correspondence of the air and water boundary layers above and below the wind waves will be investigated in the next section, from the statistical point of view.

4. Statistical features of the large-scale structure

In this section, we investigate the statistical

features of velocity fluctuations associated with the large-scale structure, which we have recognized in the previous section as the ordered motions in the water turbulent boundary layer. In order to study statistical features of the turbulence under the wind waves, Howe *et al.* (1982) and Kitaigorodskii *et al.* (1983) have separated the velocity into the turbulent part and the orbital velocity by using linear statistical techniques. In their studies, however, the energy of turbulence was not much larger than the energy of wave orbital velocity. In our experiment, the energy in the wind-wave frequencies are much smaller than the main energy of turbulence, as already shown in Figs. 7 and 8. Consequently, a low-pass filter is used simply to separate the frequency components lower than the wind-wave frequencies as the turbulence part. The filter has a very sharp characteristic as shown in Fig. 10. The cut-off frequency f_c was determined so as to filter out the frequency components near the wind-wave peak and higher than it. Therefore, the f_c depends on the wind and fetch conditions of the experiments. To designate the velocity fluctuations that resulted from this filter operation, $\hat{}$ and $\tilde{}$ are used for the lower (turbulence) and higher (wind-wave) frequency components, respectively.

The intensities of the lower (turbulence) components $(\hat{u}^2)^{1/2}$ and $(\hat{w}^2)^{1/2}$ are shown for the three wind coditions in Fig. 11(a) and the Reynolds stress $(-\hat{u}\hat{w})^{1/2}$ in Fig. 11(b). As the wind speed increases, $(\hat{u}^2)^{1/2}$, $(\hat{w}^2)^{1/2}$ and $(-\hat{u}\hat{w})^{1/2}$ increase. In each of the three wind conditions, $(\hat{u}^2)^{1/2}$, $(\hat{w}^2)^{1/2}$ and $(-\hat{u}\hat{w})^{1/2}$ have nearly constant values in the upper layer, respectively, and then decrease as depth increases. It is noticeable that, after the Reynolds stress of the three cases has decreased with depth, they reach a constant value of about 0.2; and the lower the wind speed is, the shallower the depth is at which the Reynolds stress reaches the constant value.

The turbulent velocity components at frequencies lower than the wind-wave peak frequency in the upper boundary layer have a

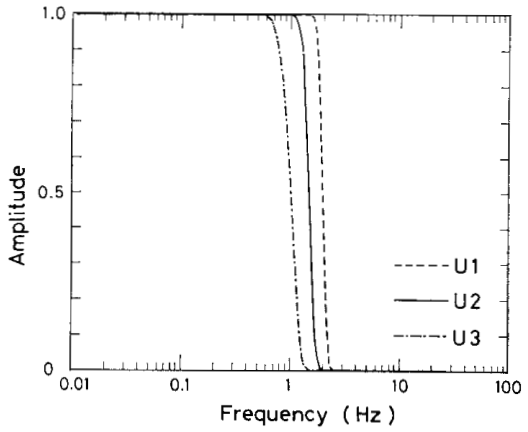

Fig. 10. Characteristics of filters used to separate the frequency components for turbulence and wind waves of the velocity fluctuations.

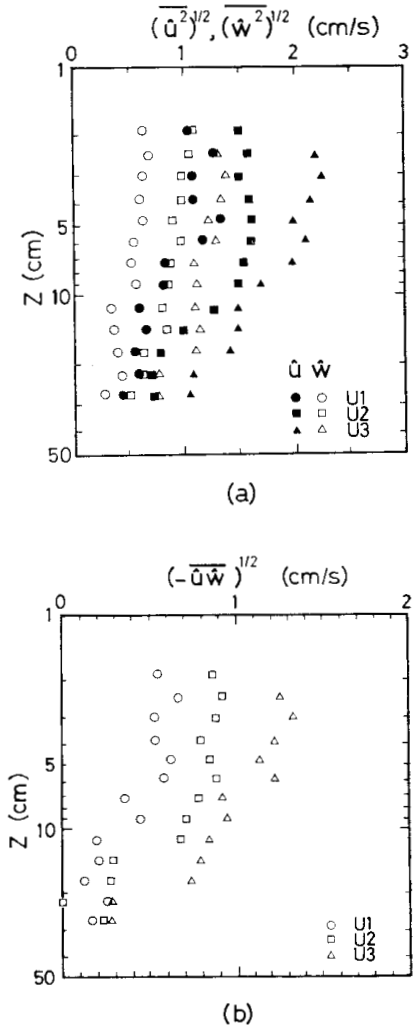

Fig. 11. (a) Profiles of $(\hat{u}^2)^{1/2}$ and $(\hat{w}^2)^{1/2}$, and (b) profiles of $(-\hat{u}\hat{w})^{1/2}$ for the three experimental conditions.

nature of constant flux and constant intensity as shown above. It is probable that the influence of the turbulence caused by energy transfer from the air flow is confined to the boundary layer near the surface ($z \gtrsim -20$ cm, depending on the wind speeds) and there is a layer filled with background low-level turbulence under this boundary layer. The under layer corresponds to the return flow region as already shown in Fig. 2.

The friction velocity u_*, which represents the momentum flux and turbulence of the air flow, was proposed as important in the self-similarity laws of growing wind waves by Toba (1972, 1973, 1978). In the present experiment, as the wind speed increases, the wind waves grow and the level of turbulence contained in the lower frequency components increases (Table 1 and Fig. 11). By using the present results, we now examine the existence of similarity structure which connects the wind waves and turbulence in water. We employ $\overline{(\eta^2)}^{1/2}\sigma_p$ as a velocity scale, and λ_p as a length scale to normalize depth, both of which represent the state of wind waves. The turbulence intensity and Reynolds stress profiles shown in Fig. 11 may be normalized by $\overline{(\eta^2)}^{1/2}\sigma_p$ and σ_p as shown in Fig. 12; scattering of the data points due to the difference of the wind speed collapses to indicate one profile for each of $\overline{(\hat{u}^2)}^{1/2}$, $\overline{(\hat{w}^2)}^{1/2}$ and $\overline{(-\hat{u}\hat{w})}^{1/2}$. These figures seem to indicate the existence of a special relationship between wind waves and water turbulence during the process of growth of the wind waves and the water turbulence. At the same time, the turbulence structure in the boundary layer has features of constant intensity and constant flux, in the normalized depth range from 0.08 to about 2/3 of λ_p for the present experimental conditions. A similar situation was also seen in the cospectra in Fig. 9.

From Fig. 12, an average value of $\overline{(-\hat{u}\hat{w})}^{1/2}/\overline{(\eta^2)}\sigma_p$ for the range of $z/\lambda_p < 2/3$ is estimated to be 0.09. Since $u_*w = \overline{(-\hat{u}\hat{w})}^{1/2}$ by definition, u_*w is estimated as $0.09 \times \overline{(\eta^2)}^{1/2}\sigma_p$. Using these values as u_*w for each of the wind conditions, the lines representing the logarithmic profile of the mean velocity $\bar{U}$ were obtained in Fig. 3 so as to fit to the streamwise velocity profiles. In Fig. 13 the data points have also been normalized in the same way as Fig. 12. The plots of the normalized data again indicate one

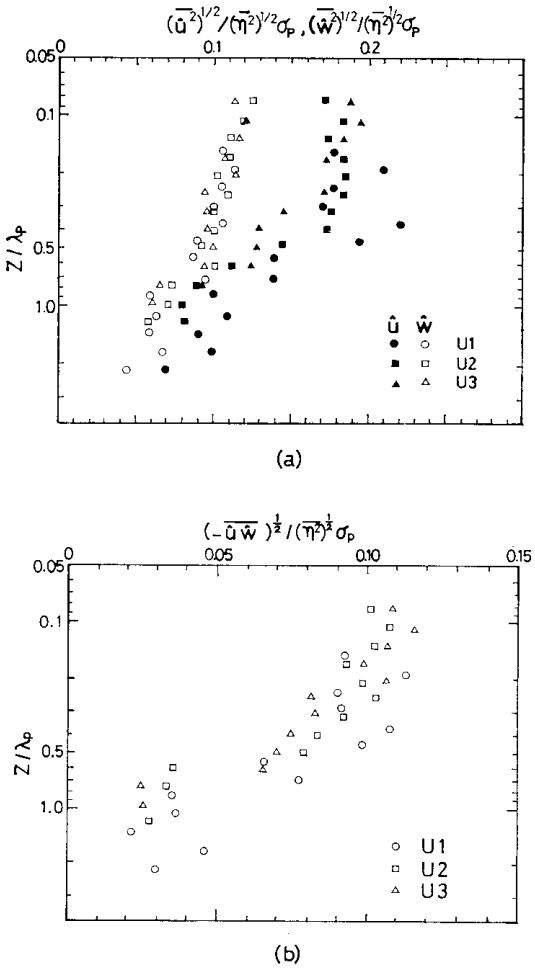

Fig. 12. Profiles of $\overline{(\hat{u}^2)}^{1/2}$, $\overline{(\hat{w}^2)}^{1/2}$, and $\overline{(-\hat{u}\hat{w})}^{1/2}$ normalized by $\overline{(\eta^2)}^{1/2}\sigma_p$. The depth is also normalized by λ_p. (a) $\overline{(\hat{u}^2)}^{1/2}$ and $\overline{(\hat{w}^2)}^{1/2}$, and (b) $\overline{(-\hat{u}\hat{w})}^{1/2}$.

line, whose inclination corresponds to the above value of u_*w, indicating the feature of the turbulent boundary layer. Two profiles of the Stokes drift velocity of wind waves, calculated by assuming $ak = 0.1$ and 0.4, are also entered in Fig. 13 for comparison. In the present experiment, $ak (\equiv \overline{(\eta^2)}^{1/2} \cdot 2\pi/\lambda_p)$ is 0.11–0.15. Here the Stokes drift $U_s(z)$ has deen calculated by

$$U_s(z) = a^2 k \exp(-2kz).$$

The Stokes drift velocity is much smaller than the measured streamwise velocity $\bar{U}$.

The amplitudes of higher frequency components $\overline{(\hat{u}^2)}^{1/2}$ and $\overline{(\hat{w}^2)}^{1/2}$ decrease exponentially

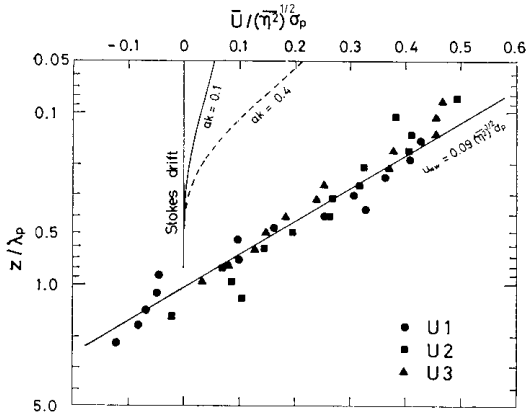

Fig. 13. Normalized profiles of mean velocity of Fig. 3. Stokes drift velocity computed for $ak=0.1$ and 0.4 is also shown for comparison.

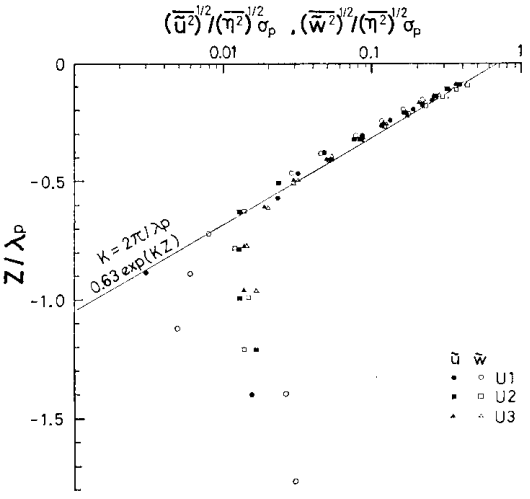

Fig. 14. Profiles of $(\overline{\tilde{u}^2})^{1/2}$ and $(\overline{\tilde{w}^2})^{1/2}$ normalized by $(\overline{\eta^2})^{1/2}\sigma_p$. The depth is normalized by λ_p.

with depth (Fig. 14). If the water waves consist of pure gravity waves of a narrow spectral band at σ_p, the coefficient of $\exp(-kz)$ should be about unity. However, the actual coefficient is 0.63 for each of three wind cases, the reason for which is discussed in Appendix 1.

The special relationship between the wind waves and water turbulence is interpreted by considering the existence of the 3/2-power law of wind waves. Namely, the 3/2-power law may be converted to $u_o=\zeta u_*$ (Toba, 1972; 1978), where u_0 is the Stokes drift velocity at the mean water surface, $U_s(0)$. Tokuda and Toba (1982) gave an experimental value of $\zeta=0.11$. By multiplying δ, the wave steepness (the wave height H divided by the wavelength λ_p), $(\overline{\eta^2})^{1/2}\sigma_p$ may converted to u_o by

$$u_0=(\pi/2)\delta\bar{H}\sigma_p$$
$$=(2.5\pi/2)\delta(\overline{\eta^2})^{1/2}\sigma_p.$$

Consequently, the normalization of $(\overline{\hat{u}^2})^{1/2}$, *etc.* by $(\overline{\eta^2})^{1/2}\sigma_p$ may be reduced to the nomalization by u_* as far δ as δ is constant, as in the case of laboratory wind waves. Also, since the boundary layer underneath wind waves is the turbulent boundary layer, $\overline{\hat{u}^2}$, $\overline{\hat{w}^2}$ and $-\overline{\hat{u}\hat{w}}$ have their respective specific ratios with u_*w, and since $u_*w\simeq(\rho_a/\rho_w)^{1/2}u_*$, Fig. 13 corresponds to the normalization of respective value sby using u_*w.

As mentioned in the introduction, many investigators have indicated that in the water boundary layer, the u_*-scaling law is satisfied, which is similar to that of the boundary layer above a solid wall. This is very natural, since the water layer underneath wind waves is also a turbulent boundary layer, and since there is the constraint of the momentum flux continuity through the air-water interface. The results of the present section demonstrate that, besides the satisfaction of the u_*-scaling law, there is a close relationship between turbulence and the wind waves at the same time. This result can be explained in view of the existence of the 3/2-power law of wind-waves. A more detailed argument on this point is given by Toba (1988) with respect to the physical interpretation of the similarity lows of wind waves.

It should be noted that, although in Fig. 12 the values of turbulence were normalized well by $(\overline{\eta^2})^{1/2}\sigma_p$ for the laboratory conditions where the wave steepness δ was nearly constant, the 3/2-power law of wind waves predicts more generally that $u_0\propto u_*$, namely that

$$(-\overline{\hat{u}\hat{w}})^{1/2}/\delta(\overline{\eta^2})^{1/2}\sigma_p,\ etc.$$

become constant in the constant flux layer of the turbulent boundary layer under wind waves. Also, the normalization of the depth, z/λ_p, should be replaced by another normalization, possibly including δ. However, the substantiation of these predictions by using data of differing values of δ in the sea is left for the future.

Acknowledgements

The authors express many thanks to Dr. Ian S. F. Jones of the University of Sydney for his stimulative discussion. They also thank Prof. H. Mitsuyasu and Dr. A. Masuda of Kyushu University for their valuable comments to the first manuscript. This study was partially supported by the Grant-in Aid for Scientific Research by the Ministry of Education, Science and Culture.

References

Antonia, R. A. (1981): Conditional sampling in turbulence measurement. Ann. Rev. Fluid Mech., **13**, 131-156.

Blackwelder, R. F. and R.E. Kaplan (1976): On the wall structure of the turbulent boundary layer. J. Fluid Mech., **76**, 89-112.

Cantwell, B.J. (1981): Organized motion in turbulent flow. Ann. Rev. Fluid Mech., **13**, 457-515.

Chen, C.H.P. and R.F. Blackwelder (1978): Large-scale motion in a turbulent boundary layer: a study using temperature contamination. J. Fluid Mech., **89**, 1-31.

Csanady, G.T. (1984): The free surface turbulent shear layer. J. Phys. Oceanogr., **14**, 402-411.

Csanady, G.T. (1985): Air-sea momentum transfer by means of short-crested wavelets. J. Phys. Oceanogr., **15**, 1486-1501.

Donelan, M.A. (1978): Whitecaps and momentum transfer. p. 273-287. *In*: Turbulent Fluxes through the Sea Surface, Wave Dynamics, and Prediction, ed. by A. Favre and K. Hasselmann, Plenum.

Howe, B.M., A.J. Chambers, S.P. Klotz, T.K. Cheung and R.L. Street (1982): Comparison of profiles and fluxes of heat and momentum above and below an air-water interface. Transaction of the ASME (J. Heat Transfer), **104**, 34-39.

Jones, I.S.F. (1985): Turbulence below wind waves. p. 437-442. *In*: The Ocean Surface, ed. by Y. Toba and H. Mitsuyasu, D. Reidel.

Jones, I.S.F. and B.C. Kenney (1977): The scaling of velocity fluctuations in the surface mixed layer. J. Geophys. Res., **82**, 1392-1396.

Kawamura, H., K. Okuda, S. Kawai and Y. Toba (1981): Structure of turbulent boundary layer over wind waves in a wind wave tunnel. Tohoku Geophys. Journ., **28**, 69-86.

Kawamura, H. and Y. Toba (1985): New aspects of the turbulent boundary layer over wind waves. p. 105-110. *In*: The Ocean Surface, ed. by Y. Toba and H. Mitsuyasu, D. Reidel.

Kawamura, H. and Y. Toba (1988): Ordered motion in the turbulent boundary layer over wind waves. J. Fluid Mech. (in press).

Kitaigorodskii, S.A., M.A. Donelan, J.L. Lumley and E.A. Terray (1983): Wave-turbulence interactions in the upper ocean. Part II: Statistical characteristics of wave and turbulent components of the random velocity field in the marine surface layer. J. Phys. Oceanogr., **13**, 1988-1999.

Mitsuyasu, H. and T. Kusaba (1985): Wind Waves and wind-generated turbulence in the water. p. 389-394. *In*: The Ocean Surface, ed. by Y. Toba and H. Mitsuyasu, D. Reidel.

Okuda, K. (1982): Internal flow structure of short wind waves. Part I. On the internal vorticity structure. J. Oceanogr. Soc. Japan, **38**, 28-42.

Rikiishi (1978): A new method for measuring the directional wave spectrum. Part II. Measurement of the directional spectrum and phase velocity of laboratory wind waves. P. Physical Oceanogr., **8**, 518-529.

Terray, E.A. and L.F. Bliven (1985): The vertical structure of turbulence beneath gently breaking wind waves. p. 395-400. *In*: The Ocean Surface, ed. by Y. Toba and H. Mitsuyasu, D. Reidel.

Toba, Y. (1972): Local balance in the air-sea boundary processes. I. On the growth process of wind waves. J. Oceanogr. Soc. Japan, **28**, 109-121.

Toba, Y. (1973): Local balance in the air-sea boundary processes. III. On the spectrum of wind waves. J. Oceanogr. Soc. Japan, **29**, 209-220.

Toba, Y. (1978): Stochastic form of the growth of wind waves in a single-parameter representation with physical implications. J. Phys. Oceanogr., **8**, 494-507.

Toba, Y. (1985): Wind waves and turbulence. p. 277-296. *In*: Recent Studies on Turbulent Phenomena, ed. by T. Tatsumi *et al.*, Assoc. for Sci., Doc. Inform., Tokyo.

Toba, Y. (1988): Similarity laws of the wind wave and a coupling process of the air and water turbulent boundary layers. Fluid Dynamics Research, **2**, 263-279.

Toba, Y., M. Tokuda, K. Okuda and S. Kawai (1975): Forced convection accompanying wind waves. J. Oceanogr. Soc. Japan, **31**, 192-198.

Tokuda, M. and Y. Toba (1982): Statistical characteristics of individual waves. II. Self-consistent similarity regime. J. Oceanogr. Soc. Japan, **38**, 8-14.

Wang, J. and J. Wu (1985): Wind-induced water turbulence. p. 401-406. *In*: The Ocean Surface, ed. by Y. Toba and H. Mitsuyasu, D. Reidel.

Appendix 1

Figure 14 shows that the amplitude of the higher frequency components $(\widetilde{u^2})^{1/2}$ and $(\widetilde{w^2})^{1/2}$

decreases exponentially with depth, though the coefficient of $\exp(-kz)$ was 0.63. As seen in the spectra in Fig. 7 (b), the energy of the higher-frequency region (2-5 Hz) is mostly due to the orbital motion of the wind waves. We expect from the linear theory of the surface gravity waves that the line of exponential decrease and the coefficient of unity for waves of such a narrow spectral band, that is;

$$\left.\begin{matrix}\overline{(\tilde{u}^2)}^{1/2}\\ \overline{(\tilde{w}^2)}^{1/2}\end{matrix}\right\}\simeq\overline{(\eta^2)}^{1/2}\sigma_p\exp(-kz). \qquad \text{(A1)}$$

Since the amplitudes were normalized by $\overline{(\eta^2)}^{1/2}\sigma_p$ in Fig. A, the coefficient of $\exp(-kz)$ becomes unity. In this appendix, we discuss the reasons for the coefficient 0.63 which is thus smaller than the expected value from linear theory.

Since the relation of Eq. (A1) can be obtained under linear monchromatic water waves, the validity of the flowmeter used here was first examined by using mechanically generated waves of frequencies, 1.19, 2.20, 2.47, 2.76 and 2.97 Hz. These frequencies cover the frequency range of the dominant wind waves in the present experiments. The amplitudes of the water velocity under the waves, normalized by $\overline{(\eta^2)}^{1/2}\sigma_p$ where subscript p has no meaning, are plotted by closed circles in Fig. A, where z is normalized by $\lambda(\sigma_p)$, which is calculated by applying $k(\sigma_p)=2\pi/\lambda(\sigma_p)=\sigma_p^2/g$. The values decrease exponentially with depth, representing the relation of Eq. (A1). This result shows that the flowmeter responds correctly to the orbital motions of water waves in these frequency ranges.

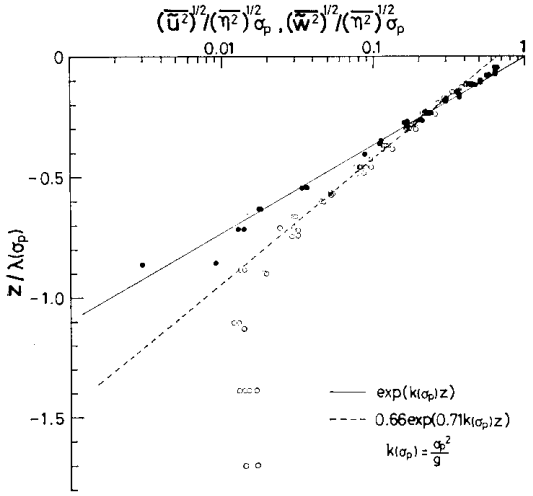

Fig. A. Profiles of $\overline{(\tilde{u}^2)}^{1/2}$ and $\overline{(\tilde{w}^2)}^{1/2}$ normalized by $\overline{(\eta^2)}^{1/2}\sigma_p$. The depth is normalized by $\lambda(\sigma_p)$. The closed circles show the velocity fluctuations under mechanically generated waves and the open circles under the wind waves.

Now we have to seek the reason of the smaller coefficient for the laboratory wind waves, assuming that the observed values are reliable. In Fig. A, $\lambda(\sigma_p)$ is used to normalize z, but λ_p, which is the wavelength obtained by using the phase difference between the two wave gauges, was used in Fig. 14. As shown in Table 1, λ_p of the wind waves are considerably greater than the $\lambda(\sigma_p)$. This tendency for the laboratory wind waves has alreaby been observed (*e.g.*, Rikiishi, 1978; Tokuda and Toba, 1982). Since the measured λ_p and the peak frequency were reliable in each case, this tendency was explained to be due to an increase of the phase speed or, equivalently, the shift of the peak frequency of the wind waves. Tokuda and Toba (1982) expressed this excess phase speed as an effective wind drift u_s.

In the present study the ratios $\lambda(\sigma_p)/\lambda_p$ of the three cases do not vary much, giving 0.73 in an average. When we plot the data of Fig. 14 in Fig. A by normalizing z with $\lambda(\sigma_p)$ (open circle), the dotted line of $0.66\exp(0.71\,k(\sigma_p)z)$ can be obtained. The value of 0.71 corresponds to that the average ratio $\lambda(\sigma_p)/\lambda_p$ is 0.73, because the data of Fig. 14 agree with the $\exp(-k_pz)$ line of a slope.

In order to normalize the amplitude of the water velocity in Section 4, we have used $\overline{(\eta^2)}^{1/2}\sigma_p$ as a representative value of the wind waves but not of the gravity waves. However when we consider only about the orbital motion for the wind waves with the wavelength λ_p, it may be reasonable to use $\sigma(\lambda_p)=(gk_p)^{1/2}$ so as to normalize the amplitude. The use of $\overline{(\eta^2)}^{1/2}\sigma(k_p)$ gives 0.85 for the coefficient of $\exp(-k_pz)$. This value is fairly close to the value expected by the linear theory, but still has a 15% discrepancy.

As well known, the wind wave has a continuous spectra and non-linear interactions between the waves exist. The wind waves are also short-crested and have directional characteristic. Even though we combined these factors, we could not explain the above discrepancy perfectly.

Okuda (1982) showed that the laboratory wind

waves have a high vorticity layer at the individual crest of wind waves. He estimated that the thickness of the vorticity layer which existed above the sinusoidal streamline of the wind waves to be about 35% of $H_{1/3}$. We may point out a possibility that the existence of the vorticity layer at the wind-wave crests contributes to produce $(\overline{\eta^2})^{1/2}$ larger than the wave height connected with the orbital motion through the linear theory. This may be another factor to cause the smaller coefficient of the $\exp(-k_p z)$.

実験室の風波下の水中の乱流構造

吉川郁夫¶, 川村　宏*, 奥田邦明**, 鳥羽良明*

要旨: 実験室の風波下の乱流構造を2成分超音波流速計と高感度サーミスタ温度計の組み合わせを用いて調べた．温度変動は，温度を passive なスカラー量として水塊の移動を検出するのに用いた．乱流エネルギーは風波の周波数域より低い帯域 (0.01-0.1 Hz) に卓越し，その帯域では乱流は非等方的である．0.2 Hz 以上の周波数帯には，速度変動では 0.2-2 Hz，温度変動では 0.2-5 Hz に −5/3 乗でスペクトル密度が減少する等方的な領域がある．これらのことは従来の他の研究と同様である．しかし，VITA 法 (variable time-averaging technique) を用いた時系列の解析によって，上記の主要乱流帯域における顕著な事象は，水面近くからの流体の下向き bursting によっていることがわかった．このように，風波下の境界層の構造は従来考えられていたように粗面固体壁上の通常の乱流境界層と類似の性質を有するが，同時に，異なる風と波の条件下でも，この乱流のエネルギーは風波の諸量とよく関係づけられることが新たにわかった．すなわち，風波下の乱流は，風波との密接な結合のもとに発達して行くものである．

* 東北大学理学部　〒980 仙台市荒巻字青葉
¶ 神戸海洋気象台　〒650 神戸市中央区中山手通 7-14-1
** 東北区水産研究所　〒985 塩釜市新浜町 3-27-5